Molecular Dynamics Simulations of the Squarate Dianion ($C_4O_4^{2-}$) in Aqueous Solution

Lucimara R. Martins,[†] Mauro C. C. Ribeiro,[‡] and Munir S. Skaf*,[†]

Instituto de Química, Universidade Estadual de Campinas, Cx.P. 6154 Campinas, SP, 13083-970, Brazil, and Laboratório de Espectroscopia Molecular, Instituto de Química, Universidade de São Paulo, Cx. P. 26077, São Paulo, SP, 05513-970, Brazil

Received: November 1, 2001; In Final Form: March 11, 2002

A molecular dynamics simulation study of the structure and dynamics of aqueous solutions of the squarate oxocarbon dianion ($C_4O_4^{2-}$) is presented. Analyses of the solute−solvent radial distribution functions and hydrogen (H)-bonding distributions indicate a well-defined hydration shell consisting of approximately 18 water molecules. About 12 of these molecules are tightly H-bonded to the oxocarbon (an average of three molecules per oxygen atom) forming a highly symmetric solute−solvent aggregate, whereas the remaining six water molecules (not bonded to the ion) are more loosely distributed above and below the oxocarbon plane. The mean residence time for molecules that are H-bonded to the solute is estimated to be larger than 20 ps, whereas molecules that are not directly bonded to the ion are frequently exchanged with the bulk and remain within the first solvation shell for times of the order of a few picoseconds. For the dynamics, we find that the translational motions projected along the squarate plane and perpendicular to it are comparable to each other. The rotational diffusion coefficients for the main symmetry axes also indicate that the spinning and tumbling motions of the oxocarbon are roughly isotropic despite the shape of the solute. The squarate is found to perform fast librational motions inside the solvente cage, with a characteristic frequency of approximately 70 cm^{-1}, in close agreement with recent experimental Raman band shape analysis. These results are discussed in the light of the hydration structure.

1. Introduction

Oxocarbons are organic compounds in which most or all of the carbon atoms are bound to carbonyl groups or their equivalents.[1] The monocyclic dianions, $C_nO_n^{2-}$ ($3 \leq n \leq 6$; see Figure 1), and their protonated forms are the most important archetypes within the oxocarbon family.[1,2] These compounds exhibit remarkable planar geometries and unique electronic structure properties.[2−8] The squaric acid ($H_2C_4O_4$) and its derivatives, in particular, are of considerable interest to practical applications in biology and advanced materials.[2] These include the squaric acid diethyl ester as a coupling reagent in the synthesis of selective antitumoral agents[9] and the squaric acid and squarate dianion ($n = 2$) as templates for controlling the assembly of stable, highly functionalized two- and three-dimensional crystalline structures.[10,11] In addition, several squaraines compounds are used as electron acceptors for nonlinear optical materials[12] and photovoltaic devices[13] because of their photochemical and photoconductive properties.[14,15]

From the spectroscopic standpoint, the oxocarbon dianions emerge as one of the few examples where, because of the degeneracy of the first singlet state, the Raman active nontotally symmetric vibrational modes derive their intensities from the Jahn−Teller effect.[16] In fact, oxocarbon dianions are excellent Raman probes. The squarate and croconate exhibit unusually high Raman intensities for both totally symmetric and nontotally symmetric modes, with relatively well-separated bands. Such a distinctive property has been used to examine the Raman line shapes of modes of different symmetries in aqueous solutions, thus providing an experimental route the reorientational dynamics about the in-plane and out-of-plane symmetry axes of the oxocarbons.[17] Detailed analyses based on the isotropic and anisotropic components of the totally symmetric ring breathing mode, along with the anisotropic parts of the nontotally symmetric C−C stretching and ring bending modes, indicate that reorientation of the oxocarbon anions is very hindered in water, with comparable decay rates for spinning and tumbling of the main symmetry axis.[17] Moreover, vibrational dephasing analysis predicted small values for the relaxation time (0.1 ps) of the vibrational frequency fluctuations. This fast modulation together with the observed slow rotational-diffusion dynamics suggests a picture where the ions undergo rapid librational motions inside solvent cages, which are continually formed and disrupted on a time scale that should exceed several times the characteristic librational period. The characteristic librational frequency for the croconate is estimated at 80 cm^{-1}.[17] Furthermore, the observed absence of inhomogeneous broadening indicates that the solvent cages should present relatively well-defined structures.

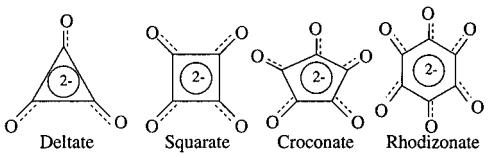

Figure 1. Molecular structures of the $n = 3-6$ monocyclic oxocarbon dianions.

The goal of the present work is to further understand the behavior of these aqueous solutions from a molecular perspective. For this purpose, we have carried out molecular dynamics

* To whom correspondence should be addressed. E-mail: skaf@iqm.unicamp.br. Fax: 55+19+3788-3023.
† Universidade Estadual de Campinas.
‡ Universidade de São Paulo.

10.1021/jp014038p CCC: $22.00
Published on Web 04/30/2002

(MD) simulations of a single $C_4O_4^{2-}$ ion in water, aiming specifically at the hydration structures, H-bonding, and dynamical properties. Our choice for the squarate among the oxocarbon anions was motivated in part by the fact that its molecular geometry is fairly rigid and planar,[16] which facilitates analysis, and in part by the considerations above. In this paper, we present simulation results for the solute−solvent H-bonding geometry and distribution and examine the effects of the oxocarbon on the H-bonding characteristics of the surrounding solvent. Analysis of a complete set of solute−solvent radial distibution functions shows the existence of a highly symmetric and stable hydration shell maintained by solute−solvent H-bonding, corroborating the physical picture suggested by the Raman measurements.[17] The persistence and composition of the first hydration shell is estimated from calculations of the mean residence time. In terms of the dynamics, we have computed translational and rotational diffusion coefficients for motions projected along the main symmetry axis and perpendicular to it, thus enabling a more direct insight into the nature of the squarate motion in water. Morevover, the fast librational motions of the anion have been studied through time correlation functions of the angular velocities and reorientation of the symmetry axes.

The remainder of this paper is organized as follows: In section 2, we present details of the simulation and force-field parameters. Our main results and discussion on the structural and dynamical properties are found in sections 3 and 4, respectively. Our concluding remarks are presented in section 5.

2. Potentials and Simulation Details

The squarate is modeled as a rigid, planar molecular ion of D_{4h} symmetry[16] in which the C−C and C−O bond lengths measure 1.47 and 1.26 Å respectively.[18] The CCC and OCC angles are 90° and 135° (see Figure 1). Both solute and solvent molecules are described by interaction-site potentials given by Lennard-Jones plus Coulumbic terms:

$$V_{ij}(r) = 4\epsilon_{ij}[(\sigma_{ij}/r)^{12} - (\sigma_{ij}/r)^{6}] + \frac{q_i q_j}{4\pi\epsilon_0 r} \qquad (1)$$

where q_i is the partial charge on site i, ϵ_{ij} and σ_{ij} are the Lennard-Jones parameters, and r is the distance between sites i and j on different molecules. For sites of different types, we used the usual Lorentz−Berthelot[19] combination rules, $\epsilon_{ij} = (\epsilon_{ii}\epsilon_{jj})^{1/2}$ and $\sigma_{ij} = (\sigma_{ii} + \sigma_{jj})/2$. The solvent is described by the well-tested SPC/E model.[20] Lennard-Jones parameters for the atoms on the oxocarbon were taken from the OPLS force-field[21] without further refinements. This is justified here in view of the lack of experimental thermodynamic or structural data that could be used as targets in a parametrization procedure for the squarate in solution. The set of Mulliken partial charges on the oxocarbon used here were obtained from the ab initio calculations of Puebla and Ha.[4] These charges are in close agreement with those obtained recently by Schleyer et al.[6] and also with our own ab initio and DFT calculations, which take into account a cluster of neighboring solvent molecules.[22]

The simulations were performed in the NVE ensemble for solutions containing one $C_4O_4^{2-}$ ion and $N = 499$ SPC/E water molecules placed in a cubic box corresponding to the solvent density at ambient conditions (0.997 g/cm^3). Lennard-Jones forces were cutoff at half the box length, and Coulomb forces were treated via Ewald sums with conducting boundaries.[23] The equations of motion were integrated with leapfrog and quaternions algorithms[19] with a time step of 1 fs. Total energy conservation is achieved within 0.5% during uninterrupted runs of 10 ps, with an average temperature of 298.8 K. Approximately 150 equilibrated 10 ps runs were used for data analysis, each separated by smaller runs (3 ps) during which the velocities were rescaled to the desired temperature of 298 K. The trajectories were discarded during velocity rescaling. In addition, a few simulations were also performed in the presence of Li^+ counterions, in which a pair of water molecules were replaced by two Li^+. The purpose of these simulations is to investigate possible effects of the counterions on the behavior of the aqueous squarate because previous experiments on the dynamics of these systems were performed using a Lithium salt.[17] The potential parameters for the Li^+ cations are taken from Pettitt and Rossky.[24] Details of the interaction potential parameters are listed in Table 1.

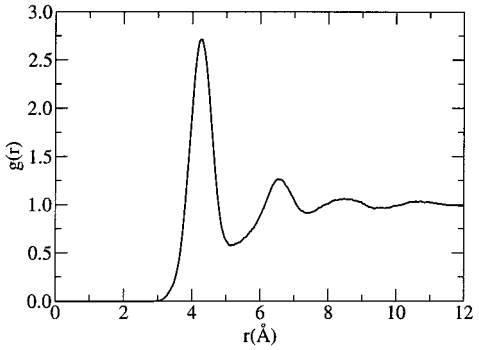

Figure 2. Solute−solvent radial distribution function involving the squarate and water center of masses. The first two local minima are located at 5.2 and 7.4 Å and define the radii of the first and second hydration shells around the anion as a whole.

TABLE 1: Potential Energy Parameters for SPC/E Water and the Squarate and Li^+ Ions Used in Our Simulations

site	σ (Å)	ϵ/k_B (K)	charge (e)
O_w	3.17	78.48	−0.8476
H	0.00	0.000	0.4238
O_x	2.96	105.68	−0.851
C	3.75	52.84	0.351
Li^+	1.39	67.08	1.000

3. Structural Properties

3.1. Hydration Structures. To discuss the hydration structures, it is necessary to introduce a suitable definition for the first, second, and possibly outer solvation shells around the squarate anion as a whole because the solute is polyatomic and nonspherical. This could be done in a number of different ways. For simplicity, the solvation shells are here defined based on the position of the local minima of the radial distribution function between the solute and solvent center of masses, which is shown in Figure 2. Accordingly, the radii of the first and second hydration shells are 5.2 and 7.4 Å, respectively. The first hydration shell comprises an average of 18.3 water molecules.

The radial distribution functions (RDFs) $g_{ij}(r)$ for the anion−water sites provide a suitable means of determining the average hydration structures in more detail. The results for all solute−solvent site−site pairs are displayed in Figure 3, where panels a−d depict the RDFs for the O_xH, O_xO_w, CH, and CO_w pairs, respectively. The first peaks of the O_xH and O_xO_w RDFs yield approximately 3.1 hydrogens and 3.2 water oxygens coordinating each O_x atom. These results indicate that roughly 12 out of the 18 water molecules comprising the first hydration shell may be H-bonded to the oxocarbon. This finding should be contrasted

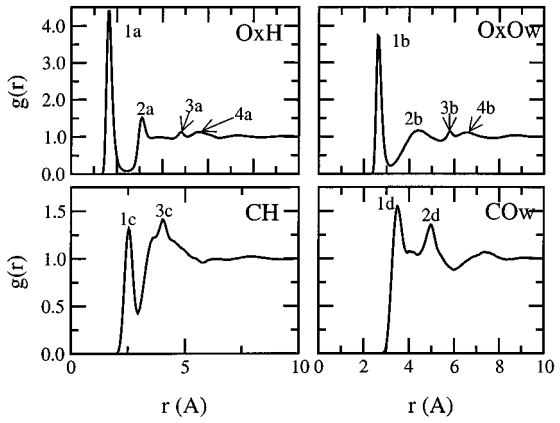

Figure 3. Solute−water site−site radial distribution functions obtained from the MD simulations. The site pairs are as indicated.

to the hydration structure deduced from MD simulations of SO_4^{2-} in water.[26] It has been found 3.3 water molecules close to each sulfate oxygen, and on average, 13.25 water molecules build the first solvation shell. In comparison to sulfate, it is clear that the particular geometry of the $C_4O_4^{2-}$ anion allows for an additional six water molecules in its first solvation shell, which are however loosely bound (see further below). On the other hand, the role played by the anion charge is illustrated by comparing with MD simulations of NO_3^- in water.[27] It has been found that 10−11 water molecules are in the first solvation shell of the nitrate, but the distribution of water is almost uniform around the anion. Further inspection of Figure 3 reveals the existence of sharply defined structures in the O_xH and O_xO_w RDFs for separations as large as 5 or 7 Å (cf. the peaks marked 3a, 4a, and 2b−4b). Such well-resolved structures stem from correlations between water molecules coordinated to different oxygen atoms of the anion.

The average structure of the first hydration shell can be built from the location of RDFs peaks using elementary geometry. The resulting structure is depicted in Figure 4a, where only six out of the approximately 18 water molecules are shown. The three hydrogen atoms (of distinct water molecules) that are H-bonded to an O_x site form an equilateral triangle lying perpendicularly to the oxocarbon plane. Each of the three $H\cdots O_xC$ angles is 120°, whereas the dihedrals $H-O_x-C_1-C_2$ are respectively −90°, +30°, and +150°. Adjacent triangles have vertexes pointing in opposite directions with respect to the squarate plane. The remaining six water molecules (not H-bonded to the solute) are scattered above and below the oxocarbon ring. The peaks labeled 1a−4b in Figure 3 can be assigned to specific average site−site distances in the Figure 4a, as summarized in Table 2. Peaks 1a−1d stem from the pairs O_x1H1 and their equivalents, peaks 3a−3c correspond to one carbonyl group with the solvent molecules surrounding an adjacent carbonyl (e.g., O_x1H9, O_x1O_w5, C1H9), and so forth. The overall characteristic of the squarate hydration structure is consistent with an electronic charge distribution with excess charge equally distributed over the oxygen atoms and carbon−oxygen bonds that are significantly resonant with the aromatic ring.[6,8,22]

During the course of the simulation, we have frequently encountered solvent configurations in which one or two of the oxocarbon oxygens are coordinated by four neighboring water molecules, whereas the other O_x atoms remain three coordinated. One of such configurations is depicted in the lower panel of Figure 4 showing an O_x atom H-bonded to four water molecules. These solvent configurations fluctuate considerably such that

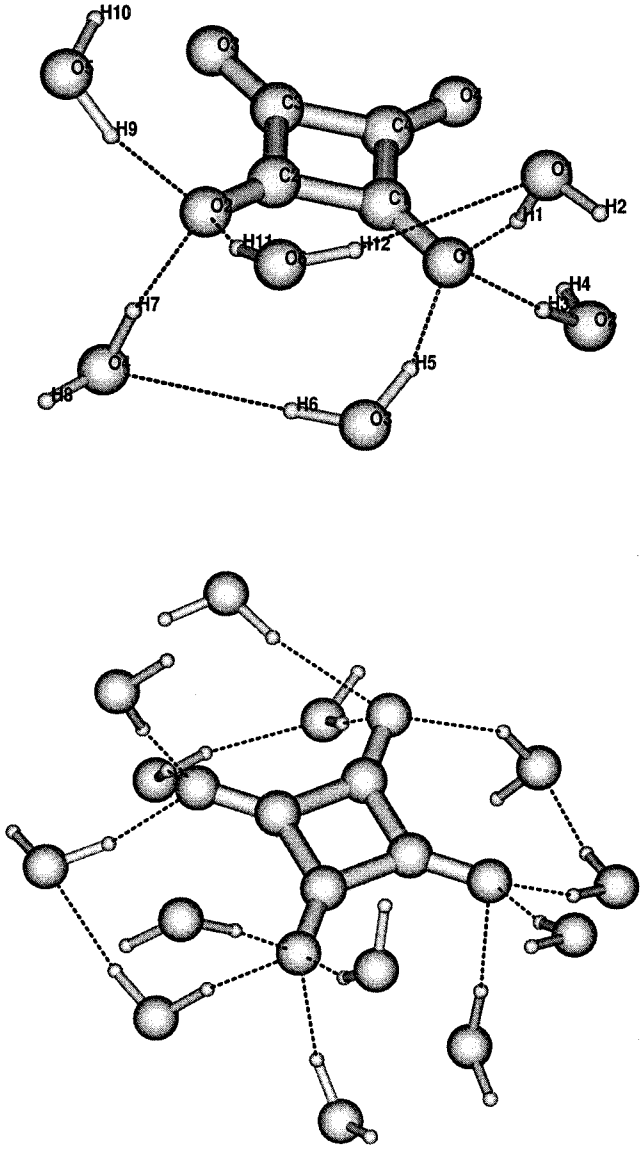

Figure 4. (a) Average structure of the squarate first hydration shell built from geometrical considerations of the RDFs. The first hydration shell consists of 18 molecules, nearly 12 of which are H-bonded to the solute (only six are shown). The water molecules not bonded to the anion are distributed above and below the oxocarbon plane (not shown). The triangles H1H3H5 and H7H9H11 point in opposite directions and, on the average, lie normal to the oxocarbon C1O1 and C2O2 bonds, respectively. (b) Snapshot of a frequently encountered MD configuration in which one of the squarate oxygens is H-bonded to four water molecules.

no features of the RDFs can be atributted to them specifically. The distribution of H bonds around the oxocarbon as a whole is examined in detail further below.

Figure 4 also indicates that there may exist H bonds between a pair of water molecules coordinating distinct carbonyl groups (e.g., the H bond $H12\cdots O_w1$). These, however, are not as long-lived as the solute−solvent H bonds. The hydrogen atoms that are not directly bonded to the solute (e.g., H12) may easily rotate because of thermal fluctuations, leading to a continuous breaking and forming of the water−water H bonds in the first hydration shell. Such dynamics remains to be investigated on a quatitative basis. Moreover, the assembly of water molecules around a given carbonyl group suggests some degree of tetrahedral ordering. To investigate to what extent the tetrahedral coordination between water molecules is preserved around the ion, the O_wO_w radial distribution function has been evaluated for

TABLE 2: Assignments of Selected Peaks in the Radial Distribution Functions of Figure 3 for the Oxocarbon−12-Water Complex[a]

peak label	position (Å)	site pair
1a	1.6	O_x1H1, O_x1H3, O_x1H5
2a	3.1	O_x1H2, O_x1H4, O_x1H6, O_x1H12
3a	4.8	O_x1H9
4a	5.6	O_x1H8, O_x1H10
1b	2.6	O_x1O_w1, O_x1O_w2 O_x1O_w3
2b	4.4	O_x1O_w4, O_x1O_w6
3b	5.8	O_x1O_w5
1c	2.5	C1H1, C1H3, C1H5
2c	3.6	C1H2, C1H4, C1H6 C1H11, C1H12
3c	4.0	C1H7, C1H9
1d	3.5	C1O_w1, C1O_w2 C1O_w3, C1O_w6
2d	5.0	C1O_w5

[a] The atoms are labeled according to Figure 4a.

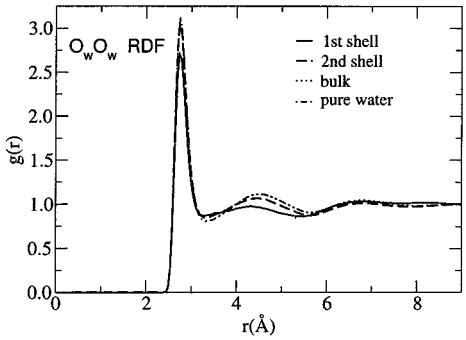

Figure 5. Radial distribution functions for water oxygens computed for different regions from the squarate center. First shell molecules are those located within 5.2 Å from the anion's center; Second shell molecules are located between 5.2 and 7.4 Å from the anion's center. Water molecules located beyond 7.4 Å from the center are defined as bulk.

different regions surrounding the anion and shown in Figure 5. First shell molecules are those located within 5.2 Å from the anion's center (cf. Figure 2), second shell molecules are located between 5.2 and 7.4 Å, whereas water molecules beyond 7.4 Å from the solute center are labeled "bulk". The oxygen RDF for pure water is also shown for comparison. The peak positions and general shape of these functions suggest that the solvent's bulk tetrahedral coordination is roughly preserved even in the immediate vicinity of the oxocarbon. Additional support to this view is provided by the water−water H-bond distribution computed for these regions, as discussed in the next section.

3.2. H-Bonding Distribution. The hydration structure of the squarate dianion determined above is primarily characterized by H bonding of the solvent to the solute oxygen sites, O_x. To determine the distribution of H bonds, we used a geometric criterion by which two molecules are considered H-bonded when (i) the distance H···O is less than 2.6 Å, (ii) the distance O···O is less than 3.5 Å, and (iii) the angle O···OH does not exceed 30°.[25] This criterion is applied to both oxocarbon−water and water−water pairs because the Lennard-Jones diameters for O_w and O_x are similar.

The distribution of O_x−water H bonds is peaked at three water molecules per oxygen atom on the squarate ion (64%), with a considerable fraction of O_x atoms bonded to four water molecules (33%) and a small fraction of two bonds (2%). The relative occurrences of one or five H bonds per solute acceptor center are negligible. The average O_x···O_w and O_x···H distances are respectively 2.6 and 1.6 Å. Different H-bond criteria may lead to somewhat different distributions, but the qualitative aspects are hardly changed for physically reasonable definitions of H bonding. In the presence of Li^+, the fractions of two, three, and four H bonds per O_x atom are 16%, 57%, and 24%, respectively. A reduction in the fractions of three and four H bonds per O_x atom and an increase in the fraction two bonds are expected because the cations compete for water molecules. However, some degree of ionic association may also play a role.

In addtion, we have computed the statistics of solute−solvent H bonding by considering the squarate as whole, that is, by determining the number of water molecules H-bonded to each one of the four O_x atoms in a given MD configuration. Let us define the symbol $[\alpha\beta\gamma\delta]$ as the fraction of solvent configurations in which the O_x1, O_x2, O_x3, and O_x4 atoms are respectively bonded to α, β, γ, and δ water molecules. The sum of all possible permutations of $[\alpha\beta\gamma\delta]$ defines the probability $f_{\alpha\beta\gamma\delta}$ of the oxocarbon being bonded to α, β, γ, and δ water molecules regardless the order of the O_x atoms (i.e., $f_{\alpha\beta\gamma\delta} = [\alpha\beta\gamma\delta] + [\beta\alpha\gamma\delta] + \cdots$). Obviously, $f_{\alpha\beta\gamma\delta} = f_{\beta\alpha\gamma\delta}$, etc. The resulting statistics are shown in Table 3. The most abundant situation is the one in which the oxocarbon has one oxygen coordinated by four water molecules while the remainder oxygens are three coordinated (f_{4333}; a total of 13 bonds). The separate contributions to f_{4333} (i.e., [4333], [3433], etc.) indicate that the "extra" (i.e., fourth) H bond is not preferentially attached to any particular O_x atom but alternates among them. The second most abundant set of configurations is the one in which two solute oxygens are coordinated by three water molecules and the other two are coordinated by four molecules (f_{3344}; only a few of its separate contributions are shown). The fraction f_{3333}, corresponding to the four squarate oxygens being *simultaneously* coordinated by three water molecules each consists of the single highest term $[\alpha\beta\gamma\delta]$ but comprises only 13.5% of all possible H-bonding configurations. This is not inconsistent with the average hydration structure of Figure 4a which is built from the *average* disposition of water molecules around the carbonyl groups, which are, overall, predominantly coordinated by three waters.

Also shown in Table 3 are the distributions of water−water H bonds for different regions from the oxocarbon center, defined in the previous section according to the position of the local minima of the radial distribution function involving the oxocarbon and water molecules center of masses, namely, first shell $r < 5.2$, second shell $5.2 < r < 7.4$, and bulk $r > 7.4$ Å. The global H-bond distribution for pure water is also shown for comparison. For molecules within the first solvation shell, the distribution is roughly symmetrical and centered at three bonds per water molecule. This reflects the fact that molecules nearest to the solute make an H bond with the oxocarbon oxygen, thus shifting the bulk distribution one unit down. Beyond the first shell, the distribution of H bonds is very close to that exhibited by pure water. These results suggest that the despite the size and shape of the solute,its presence in solution does not seem to drastically disrupt water's ubiquitous H-bonding pattern.

3.3. Mean Residence Times. The concept of the solvation shell extends beyond the average microstructure of the solvent environment described in terms of solute−solvent static correlations.[28] Knowledge about important kinetic properties regarding the exchange of solvent molecules between different solvation shells and about the diffusional processes of the solvated species through the bulk of the solution can be gained

TABLE 3: Statistics of H-Bonding between Water and the Squarate Oxygen Atoms[a]

Squarate−Water H Bonds					
f_{4333}	f_{3344}	f_{3333}	f_{3444}	f_{2334}	f_{2344}
0.384	0.308	0.135	0.074	0.038	0.023
0.102[3433]	0.060[3434]	0.135[3333]	0.020[4434]	0.005[3243]	0.003[3244]
0.100[3334]	0.055[4433]		0.019[3444]	0.005[3423]	0.003[3442]
0.093[3343]	0.043[4334]		0.018[4443]	0.004[4332]	0.003[4234]
0.089[4333]	0.041[3344]		0.017[4344]	0.004[2334]	0.002[2434]

Water−Water H Bonds					
	h_1	h_2	h_3	h_4	h_5
r < 5.2 Å	0.03	0.20	0.48	0.26	0.03
5.2 < r < 7.4 Å	0.01	0.09	0.33	0.50	0.07
r > 7.4 Å	0.01	0.08	0.32	0.52	0.07
pure water	0.01	0.08	0.31	0.53	0.07

[a] The fractions $f_{\alpha\beta\gamma\delta}$ and the symbols [$\alpha\beta\gamma\delta$] are explained in the text. Also shown are the statistics of water−water H bonds for different regions around the anion, as indicated. The fractions h_i indicate the relative incidence of i bonds per water molecule. The H-bond statistics for pure water are shown for comparison.

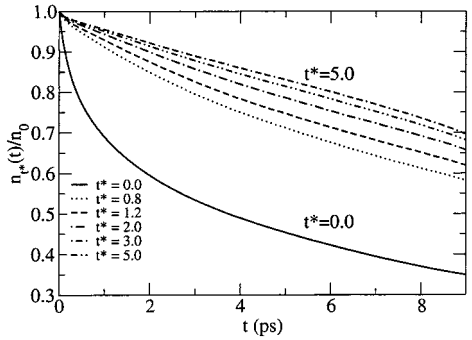

Figure 6. Normalized probability function of survival within the first hydration shell (r < 5.2 Å from the anion center) for different choice of intermittence time t^*.

from the persistence of the coordination shell, that is, from the characteristic time scale on which the solvent population in the vicinity of the solute preserves its identity. One important measure of the persistance of the coordination shell is the average time a given solvent molecule stays within an specified region around the solute, the mean residence time. A number of different definitions can be used to estimate such a parameter.[28−30] None of them, however, are direct experimental observables. In this work, the mean residence time for molecules in the first hydration shell (r < 5.2 Å, cf. Figure 2) is estimated from the decay of the survival probability function introduced by Impey, Madden, and MacDonald many years ago:[28,31]

$$\frac{n_{t^*}(t)}{n_0} = \langle \sum_{j=1}^{N} P_j(t_0, t + t_0; t^*) \rangle_{t_0} \qquad (2)$$

The function $P_j(t_0, t + t_0; t^*)$ takes on the value of 1 if the molecule j is found in the first coordination shell at times t_0 and $t + t_0$ and in the interim does not leave the coordination shell for any continuous time interval longer than t^*. $P_j(t_0, t + t_0; t^*)$ is 0 otherwise. At $t = 0$, $n_t{}^*(0) = n_0$, the average coordination number of the first shell. The survival probability function $n_{t^*}(t)/n_0$ for different choices of the intermitence time t^* calculated from the simulations are shown in Figure 6. The curves present similar decay rates for $t^* > 1$ ps. Generally for monatomic ions, $n_{t^*}(t)$ can be fit to an exponential function. In the present case, a biexponential ($a_1 e^{-t/t_1} + a_2 e^{-t/t_2}$) is needed to reasonably fit the data. Biexpoential decay is also observed for residence correlation functions of monatomic ions in methanol−water mixtures.[32] The preexponential parameters a_1 and a_2 are readily interpreted as the fraction of molecules that leave the first hydration shell within the characteristic times t_1 and t_2, respectively. Our best fitting parameters for different choices of t^* are presented in Table 4. For any given t^*, one notices the presence of "slow" (t_1) and "fast" (t_2) components in the survival probability. For $t^* = 0$, the fast component ($t_2 = 0.79$ ps) accounts for approximately 30% of the initial decay but less than 2% when $t^* = 2$ ps. This indicates that roughly 6 out of 18 water molecules do not continuously remain in the first hydration shell for times longer than ∼1 ps. For this choice of intermittence time, the average residence time for the other 12 molecules is roughly 14 ps. An inspection of the trajectories along the entire course of the simulation reveals that molecules that are not H-bonded to the anion interchange frequently between first, second, and outer solvation shells, whereas the ones that are H-bonded to the solute do not. These account for the slower components of $n_{t^*}(t)$. For $t^* > 2$ ps, the behavior of $n_{t^*}(t)$ is largely single exponential with a characteristic decay time on the order of 26 ps. This value is practically independent of the intermittence time as long as $t^* > 2$ ps and is henceforth taken as the simulated hydrodynamic mean residence time at infinite dilution.[33] In the case of the SO_4^{2-} anion, $n(t)$ presents a single-exponential decay, proper to the distinct hydration structure discussed in the previous section. As the water molecules in the first solvation shell are H-bonded to the sulfate oxigen,[26] the calculated residence time for the SO_4^{2-} (23 ps) is comparable to the slow component (t_1) of the $C_4O_4^{2-}$. These figures should be also compared to the limiting cases of simple monatomic anions, for instance, F^- and I^-, which present residence times 28.5 and 7.7 ps, respectively.[34] It is worth pointing out, however, that the average residence time around monotamic ions has been found to sharply increase for concentrated solutions.[32]

TABLE 4: Parameters of Biexponential Fits to the Survival Probability Function within the First Solvation Shell (r < 5.2 Å from the Anion Center, cf. Figure 2) for Different Choices of the Intermittence Time t^*

t^*/ps	a_1	t_1/ps	a_2	t_2/ps
0.0	0.649	14.22	0.298	0.79
0.8	0.904	20.29	0.088	1.79
1.2	0.945	21.14	0.049	1.59
2.0	0.984	22.43		
3.0	0.991	25.08		
4.0	0.993	26.11		
5.0	0.995	26.90		

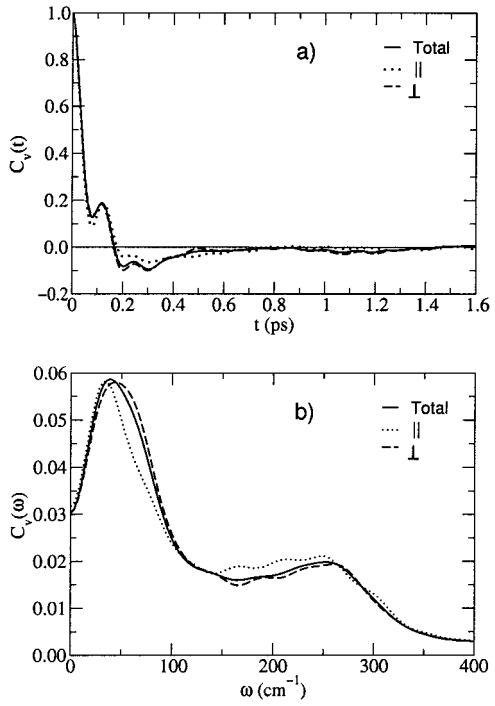

Figure 7. (a) Squarate center-of-mass normalized velocity autocorrelation function (solid line). Dotted and dashed lines stand for the projected velocities along the main symmetry axis (||) and perpendicular to it, on the oxocarbon plane (⊥), respectively. (b) The corresponding cosine Fourier spectra.

4. Dynamical Properties

4.1. Translational Dynamics. The analysis above indicates that the composition of the first hydration shell around the squarate anion persists for times significantly longer than the times associated with the translation of water molecules over a characteristic hopping distance given by the solvent intermolecular separation, $\tau_w^{trans} \sim l^2/6D_w \approx 5.7$ ps, where $l = 2.8$ Å and $D_w = 2.3 \times 10^{-5}$ cm^2/s are the position of the first peak in the O_w RDF and the self-diffusion coefficient of SPC/E water at 298K, respectively. The self-diffusion coefficient for the squarate in solution computed from the time dependence of the mean squared displacement is $D_{oxo} = 0.55 \times 10^{-5}$ cm^2/s, in the presence or absence of Li^+ counterions. This value agrees with that obtained from the velocity autocorrelation function, 0.52×10^{-5} cm^2/s. The characteristic time for translation of the anion over the typical solvent length scale is then $\tau_{oxo}^{trans} \approx$ 24 ps, which is close to the estimated mean residence time. These results combined suggest that the anion and the water molecules H-bonded to it migrate together, characterizing an ion−solvent aggregate on such time scales. Measurements of the hydrodynamic radius of the squarate in aqueous solutions are expected to reflect this feature. For comparison, the diffusion coefficients for the other mentioned anions are (in 10^{-5} cm^2/s) 1.5 (SO_4^{2-}),[26] 0.2 (NO_3^-),[27] 1.3 (F^-), and 1.7 (I^-).[34]

Further insight into the translational dynamics of the squarate in solution is gained from the anion center-of-mass velocity autocorrelation function (Figure 7a, solid line), which indicates fast oscillatory translations of the solute encapsulated by the hydration cage. The frequency spectrum of this motion as measured by the Fourier cosine transform is bimodal, with peaks approximately at 40 and 260 cm^{-1} (Figure 7b). Although we have not investigated the molecular origins of these two peaks in greater detail, our analyses suggest that the higher frequency peak corresponds to small amplitude motions of the solute relative to the first hydration shell, whereas the lower frequency component stems from the motions of the aggregate as a whole under the influence of the remainder surrounding solvent.

Figure 7 also shows the normalized auto-correlation function calculated for the projections of the center-of-mass velocity onto body-fixed directions $\hat{e}_j$ along the squarate main symmetry axis ($j = ||$; dashed line) and on the solute plane ($j = \perp$; dotted line):

$$C_v^j(t) = \frac{\langle(\hat{v}(t).\hat{e}_j).(\hat{v}(0).\hat{e}_j)\rangle}{\langle|\ \hat{v}(0).\hat{e}_j|^2\rangle} \tag{3}$$

The similarity between these correlation functions and between their frequency spectra (Figure 7b) indicates that the squarate undergoes fairly isotropic motions despite its markedly different transversal and longitudinal cross-sections. The diffusion coefficients corresponding to motions projected along and perpendicular to the main symmetry axis, computed from the time integral of $C_v^{||}$ and $C_v^{\perp}$, are 0.47 and 0.58 10^{-5} cm^2/s, respectively. The corresponding lower frequency peaks of the spectra are located at 34 and 44 cm^{-1}. These features clearly reflect the enhanced three-dimensional character of squarate-water aggregate, as depicted in Figure 4. In the absence of the indicated pattern of solute−solvent H bonding, the sliding motions of the solute plane through the solvent are considerably less hindered than translational motions projected perpendicularly to the ring. This has been verified by means of an auxiliary simulation in which the partial charges on the oxocarbon sites were set to zero.

4.2. Reorientational Dynamics. The reorientational dynamics is first examined through the angular velocity correlation function

$$C_\Omega^j(t) = \frac{\langle\hat{\Omega}_j(t).\hat{\Omega}_j(0)\rangle}{\langle|\hat{\Omega}_j(0)|^2\rangle} \tag{4}$$

depicted in Figure 8a for the components perpendicular (dashed line) and parallel (solid line) to the main symmetry axis. The correlation functions show prominent short-time oscillations, a clear indication of fast librational motions because of solute−solvent H-bonding restoring forces. It is well-known that initial relaxation of such correlation functions are given by a Gaussian decay whose characteristic time at a fixed temperature depends solely on the inertia tensor and the mean squared torque.[35,36] The early-time ($t < 0.05$ ps) relaxation for the angular velocity components around the || and ⊥ axes are very similar to each other despite the 40% difference in their moments of inertia ($I_{||} = 6.48 \times 10^{-45}$, $I_\perp = 3.24 \times 10^{-45}$ kg m^2). This means that the reorientational motions of the squarate anion in water can only be rationalized within the concept of a solute−solvent aggregate. To illustrate this point further, we have calculated $C_\Omega^{||}(t)$ and $C_\Omega^{\perp}(t)$ from the auxiliary simulations with zero site charges on the oxocarbon (Figure 8b). In the absence of strong solute−solvent association, there are no longer highly hindered librational oscillations, and the initial Gaussian decay follows the trend accordingly to the inertia tensor components ($I_{||}^{-1} < I_\perp^{-1}$).

The rotational diffusion coefficients for spinning and tumbling of the main symmetry axis, $\Theta_{||}$ and $\Theta_\perp$, are obtained from the corresponding time correlation through the relation

$$\Theta_j = \langle|\Omega_j|^2\rangle \int_0^\infty C_\Omega^j(t)\, dt; \quad j = \perp, || \tag{5}$$

We obtain $\Theta_{||} = 5.8 \times 10^{-3}$ ps^{-1} (spinning around the main symmetry axis) and $\Theta_\perp = 8.0 \times 10^{-3}$ ps^{-1} (tumbling). The

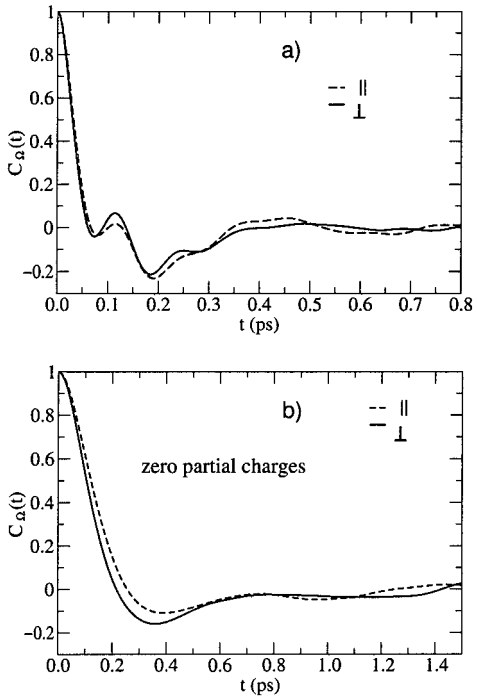

Figure 8. (a) Normalized autocorrelation functions for the angular velocity components along the main symmetry axis (spinning; dashed line) and perpendicular to it (tumbling; solid line). (b) The same, calculated for a completely apolar (ficticious) oxocarbon probe with no site charges.

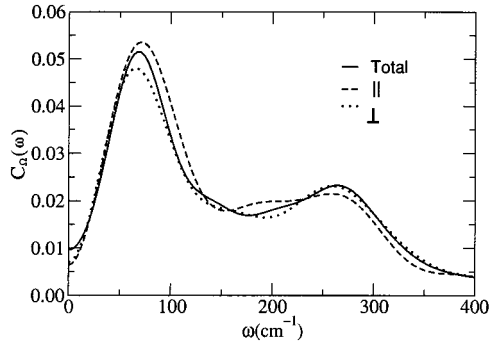

Figure 9. Cosine Fourier transforms of the angular velocity autocorrelation functions of Figure 8a versus frequency.

rotational anisotropy coefficient $\alpha = \Theta_{||}/\Theta_{\perp}$ is then approximately 0.72, indicating that tumbling of the squarate ring is somewhat faster than spinning about the main symmetry axis. This is in marked contrast with the behavior exhibited by benzene and 1,3,5-trimethylbenzene, which are also flat symmetrical rotors, but are found to be essentially free to spin in a variety of organic solvents.[37,38] The frequency spectra of the angular velocity time correlation functions are depicted in Figure 9. Like the spectra of the center-of-mass VACF, the spectra of $C_\Omega^\perp(t)$ and $C_\Omega^{||}(t)$ are bimodal, with main peaks centered about 70 cm^{-1} and secondary peaks located approximately at 270 cm^{-1}.

Closer connection with available Raman spectroscopy measurements of the reorientational dynamics is established through the time correlations $C_2^{||,\perp}(t) = \langle P_2[\hat{e}_{||,\perp}(t).\hat{e}_{||,\perp}(0)]\rangle$ for reorientation of the symmetry axes. Results for $C_2^{||}(t)$ and $C_2^{\perp}(t)$ are shown in Figure 10 (top). In the post librational regime, characterized by times $t > 0.7$ ps, both $C_2^{||}(t)$ and $C_2^{\perp}(t)$ are well described by biexponentials with fitting parameters listed in Table 5 (also shown are the components of the translational and rotational diffusion coefficients). It can be seen that the normalized reorientational time-correlation for the main symmetry axis decays faster than for a vector on the oxocarbon plane because $C_2^{||}(t)$ is not affected by the spinning of the solute, whereas the $C_2^{\perp}(t)$ time-correlation has contributions from both spinning and tumbling motions. The characteristic reorientation times obtained from integration of $C_2^{||}(t)$ and $C_2^{\perp}(t)$ are $\tau^{||} = 32$ and $\tau^{\perp} = 43$ ps, respectively. Such anisotropy of the relaxation of $C_2(t)$ has been also found in MD simulations of NO_3^- in water,[27] although the relaxation times of the (single exponential) $C_2^{||}$ and $C_2^{\perp}$ functions are much smaller: $\tau^{||} = 0.65$ and $\tau^{\perp} = 0.68$ ps. The frequency spectra, $\omega^2 C_2^{||,\perp}(\omega)$, shown in Figure 10 (bottom) exhibit features similar to those exhibited by the spectra of angular velocities. The main librational band appears again at 70 cm^{-1} followed by a less intense and broader band between 200 and 300 cm^{-1}. The main librational frequency is in good agreement with the experimental estimates from Raman scattering (80 cm^{-1}).[17] However, the secondary band at higher frenquency observed in the simulations has not yet been experimentally verified.

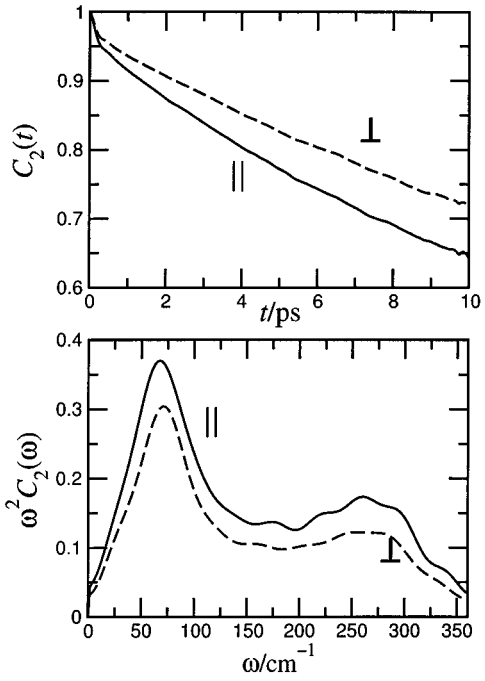

Figure 10. (a) $C_2(t)$ time-correlation functions for the reoerientation of the main symmetry axis (solid line) and of a vector on the oxocarbon plane (dashed line). (b) The corresponding cosine spectra times ω^2.

TABLE 5: Biexponential Fits to the $C_2^{||,\perp}(t)$ Functions for $t >$ 0.7 ps[a]

$D_{||}$ (10^{-5}cm^2 s^{-1})	$D_\perp$ (10^{-5} cm^2 s^{-1})	$\Theta_{||}$ (10^{-3} ps^{-1})	$\Theta_\perp$ (10^{-3} ps^{-1})
0.47	0.58	5.8	8.0

	a_1	t_1/ps	a_2	t_2/ps
$C_2^{||}$	0.194	7.33	0.765	39.54
$C_2^{\perp}$	0.196	11.27	0.772	52.10

[a] Also shown are the translational and rotational diffusion coefficients.

5. Concluding Remarks

We have carried out MD simulations of aqueous solutions containing a squarate dianion and determined the structure of the first hydration shell. We find a highly symmetric and stable

solvent cage around the anion consisting of approximately 12 or 13 water molecules H-bonded to the oxocarbon oxygens (an average of approximately three water molecules per O_x). The hydration shell is completed with six additional water molecules distributed above and below the dianion plane. We find that tetrahedral coordination is partially sustained for solvent molecules H-bonded to a given carbonyl group. As a result, the solvent structure just outside the first hydration shell appears quite preserved despite the size and shape of the oxocarbon anion. The characteristic residence time in the first hydration shell for molecules that are H-bonded to the solute is approximately 26 ps. In contrast, first solvation shell molecules that are not directly H-bonded to the solute can be interchanged with the bulk on a much faster time scale.

Because of its hydration structure, the squarate anion undergoes translational and reorientational motions that are fairly isotropic for all time scales, despite its flattened molecular shape. The short-time reorientational dynamics is characterized by $\sim$70 cm^{-1} librational motions for both spinning and tumbling of the main symmetry axis. The librational frequency is in accord with previous experimental analysis. The overall reorientational times for spinning and tumbling of the symmetry axis turn out somewhat similar to each other (32 and 42 ps, respectively). Although the Raman band shape analyses of Ribeiro et al.[17] also indicate that spinning and tumbling of oxocarbons relax at similar rates, there are no experimental data for these reorientational times for the squarate in water. On the other hand, Raman or depolarized Rayleigh scattering (DRS) and spin lattice NMR measurements with carbon-13 or oxygen-17 could be combined to yield $\tau^{\parallel}$ and $\tau^{\perp}$.[37−39] For a symmetric top, $\tau^{\perp} = \tau^{\mathrm{DRS,Raman}}$ and[38,40]

$$\tau^{\mathrm{NMR}} = \frac{1}{4}\tau^{\perp} + \frac{9}{4}\frac{\tau^{\perp}\tau^{\parallel}}{\tau^{\perp}+2\tau^{\parallel}}$$

which our simulations predict to be $\tau^{\mathrm{NMR}} \approx 37$ ps.

Acknowledgment. The financial support provided by the Brazilian agencies CNPq and FAPESP (97/13535-5 and 00/04879-7) is gratefully acknowledged.

References and Notes

(1) West, R., Ed.; *Oxocarbons*; Academic Press: New York, 1980.
(2) Seltz, G.; Imming, P. *Chem. Rev.* **1992**, *92*, 1227.
(3) Aihara, J. *J. Am. Chem. Soc.* **1981**, *103*, 1633.
(4) Puebla, C.; Ha, T.-K. *J. Mol Struct.* (*THEOCHEM*) **1986**, *137*, 171.
(5) Herndon, W. C. *J. Mol. Struct.* (*THEOCHEM*) **1983**, *103*, 219.
(6) Schleyer, P. R.; Najafian, K.; Kiran, B.; Jiao, H. *J. Org. Chem.* **2000**, *65*, 426.
(7) Quiñonero, D.; Frontera, A.; Ballester, P.; Deyà, P. M. *Tetrahedron Lett.* **2000**, *41*, 2001.
(8) Cerioni, G.; Janoschek, R.; Rappoport, Z.; Tidwell, T. T. *J. Org. Chem.* **1996**, *61*, 6212.
(9) Tietze, L. F.; Schroder, C.; Gabius, S.; Brinck, U.; Goerlach-Graw, A.; Gabius, H.-J. *Bioconjugate Chem.* **1991**, *2*, 148.
(10) Karle, I. L.; Ranganathan, D.; Haridas, V. *J. Am. Chem. Soc.* **1996**, *118*, 7128.
(11) Liebeskind, L. S.; Yu, M. S.; Yu, R. H.; Wang, J.; Hager, K. S. *J. Am. Chem. Soc.* **1993**, *115*, 9048.
(12) Pu, L. S. *J. Chem. Soc., Chem. Commun.* **1991**, *6*, 429.
(13) Kobayashi, Y.; Goto, M.; Kurahashi, M. *Bull. Chem. Soc. Jpn.* **1986**, *59*, 311.
(14) Zhao, B.; Back, M. H. *Can. J. Chem.* **1991**, *69*, 528.
(15) Merrit, V. Y.; Hovel, H. J. *Appl. Phys. Lett.* **1978**, *29*, 414.
(16) Ito, M.; West, R. *J. Am. Chem. Soc.* **1963**, *85*, 2580.
(17) Ribeiro, M. C. C.; de Oliveira, L. F. C.; Santos, P. S. *Chem. Phys.* **1997**, *217*, 71.
(18) MacIntyre, W. M.; Wekerma, M. S. *J. Chem. Phys.* **1964**, *40*, 3563.
(19) Allen, M. P.; Tildesley, D. J. *Computer Simulations of Liquids*; Oxford University Press: Clarendon Park, U.K., 1987.
(20) Berendsen, H. J. C.; Grigera, J. R.; Straatsma, T. P. *J. Phys. Chem.* **1987**, *91*, 6269.
(21) Jorgensen, W. L.; Severence, D. L. *J. Am. Chem. Soc.* **1990**, *112*, 4768.
(22) Martins, L. R.; Vazquez, P. A. M.; Skaf, M. S. *J. Mol. Struct.* (*THEOCHEM*) **2002**, *580*, 137.
(23) Perram, J. W.; de Leeuw, S. V.; Smith, E. R. *Annu. Rev. Phys. Chem.* **1986**, *37*, 245; *Proc. R. Soc. London* **1980**, *373*, 27.
(24) Pettitt, B. M.; Rossky, P. J. *J. Chem. Phys.* **1986**, *84*, 5836.
(25) See, for instance: Ladanyi, B. M.; Skaf, M. S. *Annu. Rev. Phys. Chem.* **1993**, *44*, 335 and references therein.
(26) Cannon, W. R.; Pettitt, B. M.; McCammon, J. A. *J. Phys. Chem.* **1994**, *98*, 6225.
(27) Kataoka, Y. *Bull. Chem. Soc. Jpn.* **1993**, *66*, 2478.
(28) Impey, R. W.; Madden, P. A.; McDonald, I. R. *J. Phys. Chem.* **1983**, *87*, 5071.
(29) (a) Sciortino, F.; Poole, P. H.; Stanley, H. E.; Havlin, S. *Phys. Rev. Lett.* **1990**, *64*, 1686. (b) Sciortino, F.; Fornili, S. *J. Chem. Phys.* **1989**, *90*, 2786.
(30) Koneshan, S.; Rasaiah, J. C.; Linden-Bell, R. M.; Lee, S. H. *J. Phys. Chem. B* **1998**, *102*, 4193.
(31) Garcia, A. E.; Stiller, L. *J. Comput. Chem.* **1993**, *14*, 1396.
(32) Hawlicka, E.; Swiatla-Wojcik, D. *Phys. Chem. Chem. Phys.* **2000**, *2*, 3175.
(33) Simulations performed in the presence of Li^+ couterions yield essentially the same results for the residence times.
(34) Lee, S. H.; Rasaiah, J. C. *J. Phys. Chem.* **1996**, *100*, 1420.
(35) Linden-Bell, R. M. In *Molecular Liquids: Dynamics and Interactions*, Vol. 135 of *NATO Advanced Study Institute, Series C*; Barnes, A. J., Orville-Thomas, W. J., Yarwood, J., Eds.; Reidel: Dordrecht, The Netherlands, 1984.
(36) Impey, R. W.; Madden, P. A.; McDonald, I. R. *Mol. Phys.* **1982**, *46*, 513.
(37) Alms, G. R.; Bauer, D. R.; Brauman, J. I.; Pecora, R. *J. Chem. Phys.* **1973**, *58*, 5570; **1974**, *61*, 2255.
(38) Berne, B. J.; Pecora, R. *Dynamic Light Scattering*; Dover: Mineola, NY, 2000.
(39) Gillen, K. T.; Griffiths, J. E. *Chem. Phys. Lett.* **1972**, *17*, 359.
(40) Huntress, W. T., Jr. *J. Chem. Phys.* **1968**, *48*, 3524.